***s*-PROCESS MOLYBDENUM, RUTHENIUM, AND BARIUM IN HIGH-DENSITY PRESOLAR GRAPHITE.** H. E. Bloom[1,2], T. Stephan[1,2], A. M. Davis[1,2,3], P. R. Heck[1,2,4], P. Hoppe[5], J. M. Korsmeyer[2,6], and S. Amari[7], [1]Department of the Geophysical Sciences, The University of Chicago, Chicago, IL, USA, [2]Chicago Center for Cosmochemistry, [3]Enrico Fermi Institute, The University of Chicago, Chicago, IL, USA, [4]Robert A. Pritzker Center for Meteoritics and Polar Studies, Negaunee Integrative Research Center, Field Museum of Natural History, Chicago, IL, USA, [5]Max Planck Institute for Chemistry, Mainz, Germany, [6]Department of Chemistry, The University of Chicago, Chicago, IL, USA, [7]McDonnell Center for the Space Sciences and Physics Department, Washington University in St. Louis, St. Louis, MO, USA. E-mail: bloomh@uchicago.edu.

Introduction: Following silicon carbide (SiC), graphite is the best studied type of presolar material. While an abundance of information exists regarding the isotopic compositions of C, many minor/trace elements, and some noble gases [1], numerous elements remain unexplored. Several studies have predicted and detected internal minor element refractory carbide crystals, of which Zr-, Mo-, and Ru-rich carbides have been found mostly in high density (HD) grains [e.g., 2–4]. Additional refractory elements may be present in solid solution with these carbides but have not been detected.

The goal of the present study is to measure all Mo, Ru, and Ba isotopes in presolar graphite isolated from the Murchison CM2 chondrite. These elements provide key information to better understand stellar nucleosynthesis. Here, we report on the first simultaneous detection of Mo, Ru, and Ba in presolar graphite with the Chicago Instrument for Laser Ionization (CHILI) [5]. Mo isotope compositions of presolar graphite have been previously measured using the CHARISMA instrument [6]. However, to our knowledge, the composition of Ru and Ba isotopes has not been measured in presolar graphite before.

Samples and Analytical Procedure: Five graphite grains from the Murchison KFB1 separate (2.10–2.15 g/cm^3 density, >1 µm grain size) [7] and six grains from separates G1 and G2 (nominal densities 2.2–2.3 g/cm^3 and 2.1–2.2 g/cm^3, respectively) [8] also from Murchison were analyzed in this study. The G1 and G2 grains had been previously analyzed for their C and N isotopic composition with the CAMECA NanoSIMS 50 at the Max Planck Institute for Chemistry (MPIC) in Mainz [8]. The KFB1 grains were part of a study including C and O NanoSIMS measurements at Washington University in St. Louis, He and Ne mass spectrometry at ETH Zurich, followed by Mg-Al NanoSIMS measurements at MPIC [9]. No isotope data for the KFB1 grains studied here were available, since we could only measure grains that had not been consumed in previous analyses.

CHILI utilizes resonance ionization mass spectrometry (RIMS) to measure isotopic abundances from a cloud of atoms released from a sample via desorption with a 351 nm laser focused to ~1 µm. Liberated atoms are selectively ionized with six Ti:sapphire lasers, each tuned to element-specific electronic transitions. These lasers enable CHILI to simultaneously analyze three elements with independent two-photon resonance ionization schemes. In order to separate Mo and Ru isobars at 96 u, 98 u, and 100 u, Mo and Ru ionization lasers were fired on alternate shots from the desorption laser running at 2 kHz repetition rate. Ba ionization lasers were fired together with the Ru lasers.

Results: While Mo was found associated with all analyzed graphite grains, only one grain (KFB1-G74) showed detectable amounts of Ru and Ba. Mo isotope ratios for all grains are shown in Fig. 1 as δ-values (‰-deviation from terrestrial ratios), normalized to ^{96}Mo. For KFB1-G74, we subdivided the measurement into 10 time intervals, since isotopic ratios changed drastically during the measurement while consuming the grain. While data from the first two time steps plot close to solar (in this context assumed to be identical to terrestrial) ratios, data for all subsequent intervals plot along the mixing lines that have been observed for mainstream SiC grains [10].

Ru and Ba isotopes in KFB1-G74 are highly anomalous, but no variation in isotope ratios during the measurement was found. δ-values are shown in Table 1. For some δ-values, only upper limits are given, assuming <3 counts as 95 % confidence limit, since 0 or 1 count were detected for these isotopes.

Discussion and Conclusions: All graphite grains investigated in this study show strong indication of contamination with terrestrial or solar Mo. We cannot tell whether the contamination is related to the chemicals used during grain separation from the host meteorite or is due to Murchison parent body processes.

However, graphite grain KFB1-G74 clearly showed internal Mo, which became apparent after laser desorption of the grain's surface layers. The internal Mo is strongly enriched in *s*-process isotopes, similar to Mo previously observed in presolar graphite [6], as well as in mainstream and types Y and Z SiC grains [10, 11].

Table 1. Ru and Ba isotopes in KFB1-G74 (errors are 1σ)

$\delta^{96}Ru_{100} < -944$ ‰	$\delta^{130}Ba_{136} < -448$ ‰
$\delta^{98}Ru_{100} < -833$ ‰	$\delta^{132}Ba_{136} < -407$ ‰
$\delta^{99}Ru_{100} = -871 \pm 33$ ‰	$\delta^{134}Ba_{136} = -339 \pm 120$ ‰
$\delta^{101}Ru_{100} = -855 \pm 42$ ‰	$\delta^{135}Ba_{136} = -844 \pm 23$ ‰
$\delta^{102}Ru_{100} = -578 \pm 56$ ‰	$\delta^{137}Ba_{136} = -527 \pm 34$ ‰
$\delta^{104}Ru_{100} = -924 \pm 24$ ‰	$\delta^{138}Ba_{136} = -355 \pm 25$ ‰

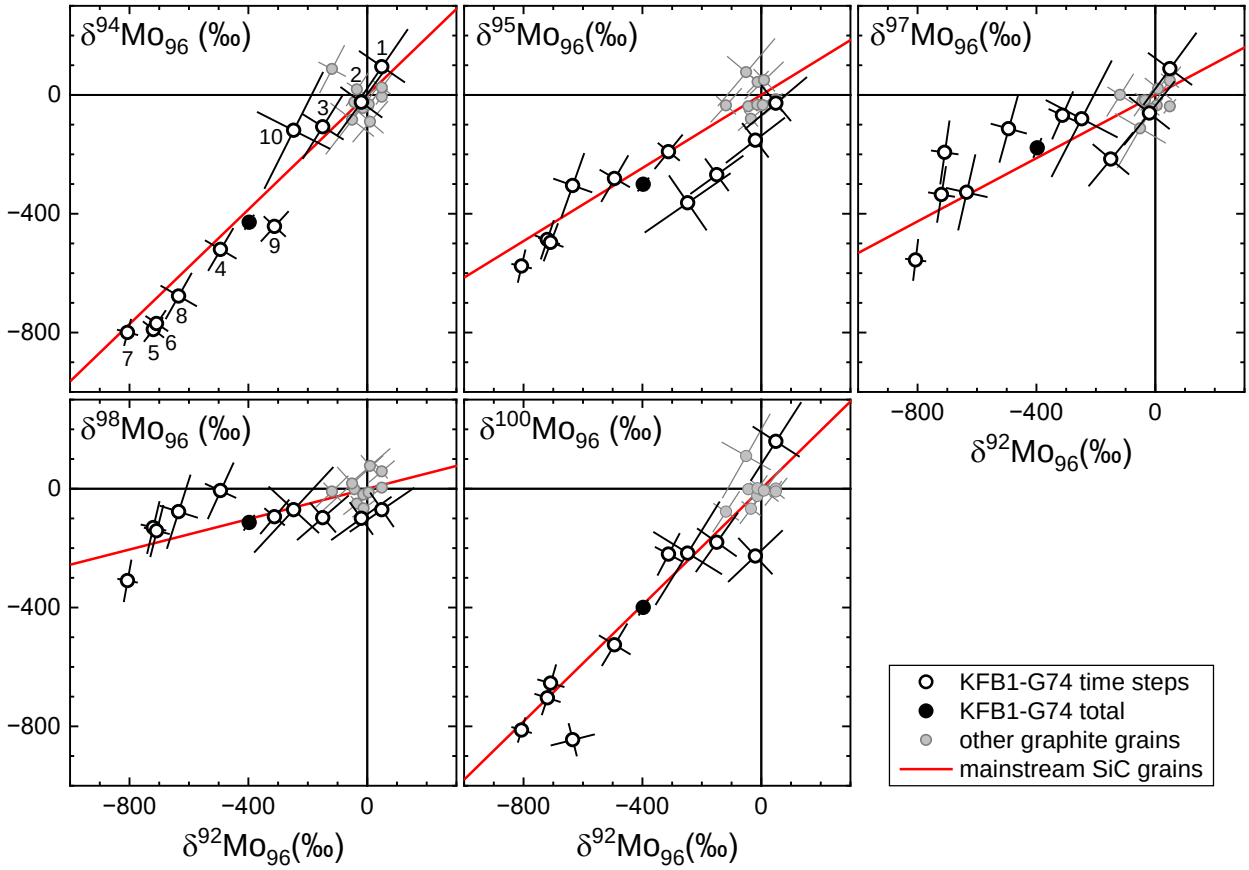

Figure 1. Mo isotope data for 11 presolar graphite grains from this study. All but one grain (KFB1-G74) show close-to-solar Mo compositions. The analysis of KFB1-G74 was divided into 10 time intervals (sequence given as numbers in the $\delta^{94}Mo_{96}$ vs. $\delta^{92}Mo_{96}$ plot). Apart from the first two steps, which show solar Mo composition, data for all other subsamples lie along typical *s*-process mixing lines, observed for mainstream SiC grains (red lines [10]). Uncertainties are 1σ.

Ru, observed here for the first time in presolar graphite, also showed an *s*-process signature in KFB1-G74, equivalent to what has recently been reported for presolar SiC grains [12]. In SiC, *s*-process enrichment in Ru was found to be directly correlated to *s*-process enrichment in Mo [12]. Since ^{92}Mo and ^{96}Ru are *p*-process-only isotopes, they have no s-process contribution; therefore, we would expect $\delta^{92}Mo_{96} = \delta^{96}Ru_{100}$, as was observed for SiC [12]. Although only an upper limit ($\delta^{96}Ru_{100} < -944$ ‰) can be given here, $\delta^{96}Ru_{100}$ is significantly lower than $\delta^{92}Mo_{96}$, which shows the lowest value of –806 ± 37 ‰ in subsample 7 of our measurement (Fig. 1). This is a clear indication that there is still some contamination contributing to the Mo isotopes even in this subsample.

Ba also showed an isotopic signature equivalent to what has been observed in mainstream SiC grains, and the isotope ratios (Table 1) exactly follow the trends described in the literature [e.g., 13–15]. It is worth mentioning that $\delta^{135}Ba_{136}$ in KFB1-G74 is among the lowest values measured in any presolar grain.

The correlated enrichment of *s*-process isotopes for Mo, Ru, and Ba in presolar graphite grain KFB1-G74 clearly link this grain to low-mass asymptotic giant branch (AGB) stars, which are also the source of mainstream and types Y and Z SiC grains. It has been suggested before that most HD graphite grains have an origin in low-metallicity AGB stars [e.g., 1].

Obviously, more data is needed, and we will continue our study of isotopic anomalies of minor elements in presolar graphite.

References: [1] Zinner E. (2014) In *Treatise on Geochemistry*, 2nd ed., Vol. 1, Elsevier, 181–213. [2] Bernatowicz T. J. et al. (1996) *ApJ*, *472*, 760–782. [3] Croat T. K. et al. (2005) *ApJ*, *631*, 976–987. [4] Croat T. K. et al. (2008) *MAPS*, *43*, 1497–1516. [5] Stephan T. et al. (2016) *Int. J. Mass Spectrom.*, *407*, 1–15. [6] Nicolussi G. K. et al. (1998) *ApJ*, *504*, 492–499. [7] Amari S. et al. (1994) *GCA*, *58*, 459–470. [8] Hoppe P. et al. (2009) *LPS*, *40*, #1010. [9] Heck P. et al. (2009) *ApJ*, *701*, 1415–1425. [10] Stephan T. et al. (2019) *ApJ*, *877*, 101. [11] Liu N. et al. (2019) *ApJ*, *881*, 28. [12] Stephan T. et al. (2021) *MAPS*, *56*, A252 (#6270). [13] Liu N. et al. (2014) *ApJ*, *786*, 66. [14] Liu N. et al. (2015) *ApJ*, *803*, 12. [15] Stephan T. et al (2018) *GCA*, *221*, 109–126.